Intravital imaging identifies VEGF-TXA_2 axis as a critical promoter of PGE_2 secretion from tumor cells and immune evasion.

Yoshinobu Konishi[1, 2, 5, 6, 7], Hiroshi Ichise[1], Tetsuya Watabe[2], Choji Oki[3], Shinya Tsukiji[3], Yoko Hamazaki[4], Yasuhiro Murakawa[5], Akifumi Takaori-Kondo[6], Kenta Terai[1,*], and Michiyuki Matsuda[1, 2]

[1]Laboratory of Bioimaging and Cell Signaling, Graduate School of Biostudies, Kyoto University, Kyoto 606-8501, Japan

[2]Department of Pathology and Biology of Diseases, Graduate School of Medicine, Kyoto University, Kyoto 606-8501, Japan

[3]Department of Nanopharmaceutical Sciences, Nagoya Institute of Technology, Nagoya 466-8555, Japan

[4]Department of Life Science Frontiers, Center for iPS Cell Research and Application, Kyoto University, Kyoto 606-8507, Japan

[5]RIKEN-IFOM Joint Laboratory for Cancer Genomics, RIKEN Center for Integrative Medical Sciences, Yokohama 230-0045, Japan

[6]Department of Hematology and Oncology, Graduate School of Medicine, Kyoto University, Kyoto 606-8507, Japan

[7]Department of Hematology, Kansai Electric Power Medical Research Institute, Osaka 553-0003, Japan

*Lead Contact and Correspondence author: Kenta Terai, Laboratory of Bioimaging and Cell Signaling, Graduate School of Biostudies, Kyoto University, Yoshida-Konoe-Cho, Sakyo-ku, Kyoto 606-8501, Japan. Phone: 81-75-753-9450; Fax: 81-75-753-4655; E-mail: terai.kenta.5m@kyoto-u.ac.jp

Abstract

Prostaglandin E_2 (PGE_2) promotes tumor progression through evasion of anti-tumor immunity. In stark contrast to cyclooxygenase-dependent production of PGE_2, little is known whether or not PGE_2 secretion is regulated within tumor tissues. Here, we show that VEGF-dependent release of thromboxane A_2 (TXA_2) triggers Ca^{2+} transients in tumor cells, culminating in PGE_2 secretion and immune evasion. Ca^{2+} transients cause cPLA2 activation and trigger arachidonic acid cascade. Therefore, we monitored Ca^{2+} transients as the surrogate marker of PGE_2 secretion. Intravital imaging of $Braf^{V600E}$ mouse melanoma cells revealed that the proportion of cells exhibiting Ca^{2+} transients is markedly higher in melanoma cells implanted into mice than those *in vitro*. We found that TXA_2 receptor is indispensable for the Ca^{2+} transients *in vivo*, and high intra-tumoral PGE_2 concentration and evasion of anti-tumor immunity. Motesanib, a vascular endothelial growth factor (VEGF) receptor antagonist, rapidly suppressed Ca^{2+} transients and reduced TXA_2 and PGE_2 concentrations in tumor tissues. These results identify VEGF-TXA_2 axis as a critical promoter of PGE_2-dependent tumor immune evasion, providing a molecular basis underlying the immunomodulatory effect of anti-VEGF therapies.

Key words

PGE_2, Immune evasion, Tumor microenvironment, Intravital imaging, Calcium imaging, GPCR, Gq signaling, TXA_2, VEGF

Introduction

Tumor cell-derived prostaglandin E_2 (PGE_2), a cyclooxygenase (COX) metabolite of arachidonic acid, promotes tumor progression by a number of mechanisms that modulate cell growth, invasion, migration, angiogenesis, immune evasion, and so on (1-3). Even if we limited ourselves to anti-tumor immunity, PGE_2 inhibits at least three cell types, NK cells, conventional type 1 dendritic cells (cDC1), and cytotoxic T cells (4-8). Currently, it is believed that the concentration of PGE_2 within tumor tissues is regulated mostly, if not entirely, by transcriptional regulation of proteins that constitute the pathways for the synthesis, transport, and degradation of PGE_2 (9). Among them, the cyclooxygenases COX-1 and COX-2, which are encoded by *PTGS1* and *PTGS2*, respectively, have been studied most extensively because of the established roles of nonsteroidal anti-inflammatory drugs (NSAIDs), inhibitors of COX, in the prevention of tumorigenesis (3).

PGE_2 synthesis starts from the activation of phospholipase A2 (PLA2), which liberates arachidonic acid from cell membrane phospholipids (10). Arachidonic acid is then oxygenated by COX to yield PGH_2, which is the substrate of prostaglandin E synthases. The product, PGE_2, is secreted extracellularly and then binds to the G protein-coupled receptors (GPCRs) on the plasma membrane, designated as EP1, EP2, EP3, and EP4 (11,12). Through their association with G_s, EP2 and EP4 connect PGE_2 to the protein kinase A (PKA) pathway. Currently, it is believed that the activity of the arachidonic acid cascade is regulated by PLA2s, particularly cytoplasmic cPLA2α, during inflammation (10,13). cPLA2α is activated primarily by the elevation of cytoplasmic Ca^{2+} concentration, and to a lesser extent by other mechanisms (13,14). Curiously, despite its obvious importance in tumorigenesis, the regulation of PGE_2 production and secretion from tumor cells in the tumor microenvironment (TME) remains largely elusive.

Thromboxane A_2 (TXA_2) synthesis also starts from the COX metabolite, PGH_2, which serves as the substrate of thromboxane A synthase (12). Similarly to PGE_2, TXA_2, a potent pro-coagulant, has been implicated in many facets of tumorigenesis, including tumor growth,

angiogenesis and metastasis (3). TXA_2 is generated primarily by platelets but also by other cell types, including endothelial cells (15). Low-dose aspirin, which preferentially inhibits COX-1 to reduce TXA_2 production in platelets, decreases the risk of not only myocardial infarction, but also metastatic cancer, suggesting that COX inhibitors affect tumor cells both indirectly, by means of inhibition of platelets and coagulation cascades, and directly (16). However, our knowledge of the effect of TXA_2 is limited mostly to endothelial cells and hematopoietic cells, leaving unanswered the question of whether TXA_2 can directly influence tumor cells.

Recent advances in intravital imaging of mice are providing new avenues to study real-time intercellular communications in their native environment within various types of tumors and organs (17-20). The application of intravital imaging to the research field of tumor biology has provided several important and unprecedented views of the interplay between tumor cells and host stromal cells within the tumor microenvironment, which would not be possible with conventional *in vitro* studies (21-23). Moreover, the development of genetically encoded biosensors has led to studies clarifying the dynamics of molecular activities in association with the behavior of tumor cells and host cells (24,25).

Here, we explored whether the PGE_2 secretion from tumor cells is regulated through intercellular communications. Using distinct approaches including intravital imaging with genetically encoded calcium indicators and a bright bioluminescence imaging system with Akaluc luciferase (26), we found that PGE_2 secretion from tumor cells is indeed regulated, and that TXA_2 binds to and activates tumor cells to trigger Ca^{2+} transients and subsequent PGE_2 secretion, culminating in tumor immune evasion. Vascular endothelial growth factor (VEGF) receptor antagonist, motesanib, significantly suppressed Ca^{2+} transients with marked reduction in intra-tumoral TXA_2 and PGE_2 concentrations, demonstrating the indispensable role of VEGF receptor signaling in PGE_2-dependent tumor immune evasion.

Materials and Methods

Plasmids

Plasmids encoding GCaMP6s (27) and tdTomato (28) were obtained from Addgene (plasmid #40753; Cambridge, MA) and Takara Bio (#632533; Kusatsu, Japan), respectively. The plasmid encoding AKAR3EV was reported previously (29,30). Briefly, from the N terminus, AKR3EV consists of YPet, which is a FRET-prone variant of YFP, a spacer (Leu-Glu), the FHA domain of yeast Rad53 used as ligand domain, a spacer (Gly-Thr), an EV linker, a spacer (Ser-Gly), the consensus peptide of protein kinase A (PKA) phosphorylation (LRRATLVD) used as the sensor domain, a spacer (Gly-Gly-Arg), nTurquoise-GL (31), and the nuclear export sequence of the HIV-1 rev protein (LQLPPLERLTLD). The plasmid encoding hM3D DREADD fused with mCherry (Addgene plasmid #50460) was provided by Dai Watanabe (Kyoto University, Kyoto, Japan) (32). The plasmid encoding Venus-Akaluc was provided by Atsushi Miyawaki (RIKEN Brain Science Institute, Wako, Japan) (26). pCSIIbsr-GCaMP6s and pCSIIbsr-AKAR3EV, the lentiviral vectors for GCaMP6s and AKAR3EV, were constructed by inserting the cDNA encoding GCaMP6s and AKAR3EV into pCSII-based lentiviral vectors (33) with IRES-*bsr* (blasticidin S-resistance gene). psPAX2 (Addgene Plasmid #12260) and pCMV-VSV-G-RSV-Rev (provided by Hiroyuki Miyoshi, RIKEN BioResource Center, Tsukuba, Japan) were used for the lentivirus production. pPBbsr-GCaMP6s and pPBbsr-tdTomato were constructed by inserting cDNAs encoding GCaMP6s and tdTomato, respectively, into pPBbsr vector, a PiggyBac transposon vector, with IRES-*bsr* (34). To generate pPBbsr-hM3D-mCherry-NLS, cDNAs encoding hM3D and mCherry fused with the nuclear localization signal (NLS) of the SV40 large T antigen (PKKKRKV) were connected with cDNAs of the self-cleaving P2A peptide (35). Then, the resultant DNA nucleotides was inserted into the same pPBbsr vector. pCMV-mPBase was provided by Kosuke Yusa (Kyoto University, Kyoto, Japan). When needed, the blasticidin-resistance gene (*bsr*) in pPBbsr vector was replaced with the hygromycin-resistance gene (*hph*). To generate pT2ADW-NFAT-RE-Venus-Akaluc and pT2ADW-cAMP-

RE-Venus-Akaluc, a cDNA encoding Venus-Akaluc was inserted into the pT2ADW vector, which is a Tol2 transposon vector (36). Then, annealed oligo-DNA containing a minimal promoter (MinP) and either three NFAT response elements (NFAT-RE) (GGAGGAAAAACTGTTTCATACAGAA) or three cAMP response elements (cAMP-RE) (TGACGTCA) was inserted upstream of Venus-Akaluc (37-39). pCS-TP was provided by Koichi Kawakami (Research Organization of Information and Systems National Institute of Genetics, Shizuoka, Japan) (40). For the gene knockout, lentiCRISPR v2 vector (Addgene, #52961) was used. When needed, the puromycin-resistance gene (*pac*) in lentiCRISPR v2 vector was replaced with the hygromycin-resistance gene (*hph*).

Reagents

The inhibitors were as follows: PF-04418948 (Cayman Chemical Company, Ann Arbor, MI) as a PGE_2 receptor subtype EP2 antagonist; ONO-AE3-208 (Cayman Chemical Company) as a PGE_2 receptor subtype EP4 antagonist; flurbiprofen axetil (Flurbiprofen) (KAKEN Pharmaceutical, Tokyo) as a COX inhibitor; YM-254890 (FUJIFILM WAKO Pure Chemical Corporation, Osaka, Japan) as a Gq inhibitor; verapamil hydrochloride (Verapamil) (Eisai, Tokyo) as a calcium channel blocker; dasatinib (AdooQ BioScience, Irvine, CA) as a tyrosine kinase inhibitor; SQ29548 (Cayman Chemical) as a TXA_2 receptor (TP) antagonist; and motesanib (CHEMIETEK, Indianapolis, IN) as a VGEF receptor antagonist. I-BOP (Cayman Chemical Company) was applied for TP stimulation. Clodronate liposome (Hygieia Bioscience, Osaka, Japan) was applied for *in vivo* macrophage depletion. Arachidonic acid and recombinant human VEGF 165 protein were obtained from and MP Biomedicals, Inic. (Irvine, CA) and R&D systems (Minneapolis, MN), respectively. Akalumine-HCl, also called TokeOni, was obtained from Kurogane Kasei Co., Ltd. (Nagoya, Japan) or synthesized as previously described (41), and used as the substrate of Akaluc.

Antibodies

The following antibodies were applied for *in vivo* cell depletion: anti-asialo GM1 (FUJIFILM WAKO Pure Chemical Corporation) for NK cells, anti-Ly6G (1A8) (BioLegend) for neutrophils, and anti-CD42b (GPIbα) (R300) (Emfret, Eibelstadt, Germany) for depletion of platelets.

Cell lines

The $Braf^{V600E}$ melanoma cell line was provided by Reis e Sousa at the Francis Crick Institute (42). The breast cancer cell line 4T1 was purchased from ATCC (Manassas, VA). Madin-Darby canine kidney (MDCK) cells were purchased from the RIKEN BioResource Center (no. RCB0995). Human umbilical vein endothelial cells (HUVEC) were purchased from the Lonza Group, Ltd (Basel, Switzerland). $Braf^{V600E}$ melanoma cells and 4T1 breast cancer cells were cultured in RPMI medium (Thermo Fisher Scientific) containing 10% FBS (Sigma-Aldrich, St. Louis, MO), 100 units/ml penicillin and 100 μg/ml streptomycin (penicillin-streptomycin mixed solution; Nacalai Tesque, Kyoto, Japan). MDCK cells were cultured in D-MEM (FUJIFILM WAKO Pure Chemical Corporation) supplemented with 10% FBS (Sigma-Aldrich, St. Louis, MO), 100 units/ml penicillin and 100 μg/ml streptomycin (penicillin-streptomycin mixed solution; Nacalai Tesque). HUVECs were cultured in EGM-2 Endothelial Cell Growth Medium-2 bulletkit (Lonza Group, Ltd) including 2% FBS and used between passage 5 to 7.

Establishment of stable cell lines

To prepare the lentivirus, pCSIIbsr-GCaMP6s or pCSIIbsr-AKAR3EV was co-transfected with psPAX2 and pCMV-VSV-G-RSV-Rev into Lenti-X 293T cells (Clontech, Mountain View, CA) by using Polyethylenimine “Max” (Mw 40,000; Polysciences, Warrington, PA). Virus-containing media were harvested 48 to 72 hours after transfection, filtered, and used to infect $Braf^{V600E}$ melanoma cells or MDCK cells. For PiggyBac transposon-mediated gene transfer, pPBbsr2-tdTomato, pPBbsr2-GCaMP6s, and pPBbsr2-hM3D-mCherry-NLS were co-transfected

with pCMV-mPBase into Braf^{V600E} melanoma cells and 4T1 breast cancer cells by using Lipofectamine 3000 reagent (Thermo Fisher Scientific). For Tol2 transposon-mediated gene transfer, pT2ADW-NFAT-RE-Venus-Akaluc and pT2ADW-cAMP-RE-Venus-Akaluc was co-transfected with pCS-TP into Braf^{V600E} melanoma cells. Cells were selected with 10 μg/ml blasticidin S (InvivoGen, San Diego, CA).

CRISPR/Cas9-mediated establishment of KO cell lines

For CRISPR/Cas9-mediated KO of several genes, single guide RNAs (sgRNA) were designed using the CRISPRdirect program (43). The targeting sequences are listed in the following table. Annealed oligo DNAs for the sgRNAs were cloned into the lentiCRISPR v2 vector. The sgRNA/Cas9 cassettes were introduced into cells by lentiviral gene transfer. Infected Braf^{V600E} melanoma cells or 4T1 breast cancer cells were selected by 3 μg/ml puromycin (InvivoGen) or 200 μg/ml hygromycin B (FUJIFILM WAKO Pure Chemical Corporation). Cells were subjected to single cell cloning and examined for knockout by nucleotide sequencing. Braf^{V600E} melanoma cells expressing Cas9 (Cas9-alone) were established by lentiviral gene transfer of Cas9, using lentivirus prepared from the lentiCRISPR v2 vector without sgRNA.

Design of sgRNAs for CRISPR/Cas9-mediated gene knockout.

Gene	Targeting sequence
Ptgs1	TTACTATCCGTGCCAGAACC**AGG**
Ptgs2 (C57BL/6N)	AGATGACTGCCCAACTCCCA**TGG**
Ptgs2 (BALB/c)	TCCAATCCATGTCAAAACCG**TGG**
Gnaq	**CCT**CTGTGATTCTGTTCTTAAAC
Ptger1	**CCT**AGCGGATGAGGCAGCAACGT
Tbxa2r	ATGGCCTCTGAGCGCTTCGT**GGG**
Ptgfr	**CCA**CCTTATCAACGGAGGCATAG
Tbxas1	GCACAAAGGAACCACCCCAA**AGG**

Introduction of *Gnaq* into Gnaq KO cells

The cDNA library of $Braf^{V600E}$ melanoma cells was constructed with an RNeasy Mini Kit (QIAGEN, Hilden, Germany) and PrimeScript II 1st strand cDNA Synthesis Kit (Takara Bio). The cDNA of *Gnaq* was cloned, and then a silent mutation was introduced into the sgRNA-targeted region by overlap extension PCR. The sgRNA targeting sequence in *Gnaq* was changed from 5'-TCCTCTGTGATTCTGTTCTTAAAC-3'to 5'-AGTAGCGTCATCTTATTTCTGAAT-3'. The resultant cDNA was inserted into the pPBbsr vector and transferred into $Gnaq^{-/-}$ $Braf^{V600E}$ melanoma cells.

Mice

C57BL/6NCrSlc mice, BALB/cCrSlc mice, and BALB/c *nu/nu* mice (nude mice) were purchased from SHIMIZU Laboratory Supplies (Kyoto, Japan). NOD/Shi-scid, IL-2RγKO Jic mice (NOG mice) were purchased from In-Vivo Science International Inc. (Tokyo). Mice were housed in a specific pathogen-free facility and received a routine chow diet and water *ad libitum*. Female mice at the age of 7 to 11 weeks were used. The animal protocols were reviewed and approved by the Animal Care and Use Committee of Kyoto University Graduate School of Medicine (MedKyo20081).

Tumor cell injections

Cells were harvested by trypsinization, washed three times with PBS, and injected subcutaneously into the flank of recipient mice at 2×10^5 cells in 100 μl of 50% Matrigel (Corning, Corning, NY) in PBS. Tumor growth was measured every 2 to 3 days using a digital caliper. Because of the oval shape of the tumors and the wavy surface, the values of length x width were calculated (mm^2). For COX inhibition, flurbiprofen axetil was administered intraperitoneally (i.p.) at 25 mg/kg daily from day 0. For Gq inhibition, YM-254890 was

administered subcutaneously (s.c.) at the opposite side of the tumor at 0.5 mg/kg daily from day 0.

Quantification of PGE_2 and TXA_2

PGE_2 and TXB_2 concentrations in tumor tissues were quantified by enzyme-linked immune-sorbent assay (ELISA) essentially as described previously (44). Tumor tissues were resected 4 days after inoculation of tumor cells. These tissues were snap-frozen in liquid nitrogen and kept at -80 ºC until use. All these procedures were completed within 30 seconds. The average weight of tumor tissues was 18±4.8 mg (n = 28 mice). Tumor tissues were homogenized in the homogenization buffer [0.1 M phosphate buffer, pH 7.4, 1 mM EDTA, and 10 μM indomethacin (FUJIFILM WAKO Pure Chemical Corporation)] at a concentration of 2 ml/gram tumor using Ultra Sonic Homogenizer UH-50 (SMT corporation, Tokyo, Japan). After centrifugation at 8,000 x g for 10 minutes, the supernatants were diluted 500 or 2000 times, and subjected to ELISA for PGE_2 or TXB_2 according to the manufacturer's protocol (Enzo Life Sciences, Farmingdale, NY). In some experiments, 75 mg/kg motesanib (CHEMIETEK) were intravenously administrated 90 minutes before the resection of tumor tissues. The concentration of TXB_2 was regarded as that of TXA_2 because of the rapid inactivation of TXA_2 under physiological conditions.

TXA_2 secretion from HUVECs was also quantified by ELISA as described previously (45). HUVECs were serum starved overnight in serum-free DMEM (Nacalai Tesque). Fresh serum-free DMEM with 1 μM arachidonic acid was added one hour prior to VEGF treatment (100 ng/ml). VEGF receptor antagonist, motesanib, was added to a final concentration of 100 nM 15 minutes prior to VEGF treatment. After 20 minutes of treatment, the culture media were collected and subjected to ELISA for TXB_2 to according to the manufacturer's protocol (Cayman Chemical Company).

Time-lapse imaging by wide-field microscopy under *in vitro* conditions

Intracellular Ca^{2+} concentrations in $Braf^{V600E}$ melanoma cells were visualized with a genetically encoded calcium indicator, GCaMP6s. Briefly, the cells were imaged with an IX83 inverted microscope (Olympus, Tokyo) equipped with a UPlanSApo 40x/0.95 objective lens (Olympus), a DOC CAM-HR CCD camera (Molecular Devices, Sunnyvale, CA), a Spectra-X light engine (Lumencor Inc., Beaverton, OR), and an IX3-ZDC laser-based autofocusing system (Olympus), and a stage top incubator (Tokai Hit, Fujinomiya, Japan). The filters and dichromatic mirrors used for time-lapse imaging under *in vitro* conditions were as follows: a 438/24 excitation filter (incorporated in the Spectra-X light engine), an FF458-Di02-25x36 (Semrock, Rochester, NY) dichromatic mirror, and FF01-542/27-25 (Semrock) emission filter. To analyze the dynamics of intracellular Ca^{2+} concentration, acquired images were subjected to drift correction with Auto Align and Align Stack functions. Then, a median-filter and Open-close-filter were applied for noise reduction. The fluorescence time course was measured by averaging all pixels within the region of interest (ROI). The GCaMP intensity was quantified as the ratio of the fluorescence intensity at each time point to the fluorescence intensity at the minimum intensity projection over 10 minutes within the ROI. To smooth a data set, the averaged value of five successive time frames was adopted. To stimulate TP, 10 to 500 nM I-BOP (Cayman Chemical Company) were added to the media after more than 24 hours serum starvation.

Analysis of PKA activity in MDCK cells by wide-field fluorescence microscopy

For analysis of the PKA activity in MDCK cells, $Braf^{V600E}$ melanoma cells expressing hM3D receptor and MDCK cells expressing AKAR3EV were seeded in a 96-well plate (1:400) and imaged with an IX83 inverted microscope (Olympus) equipped with an UPLSAPO 20X objective (Olympus), a Prime sCMOS camera (Photometrics), a CoolLED precis Excite light-emitting diode (LED) illumination system (Molecular Devices), an IX2-ZDC laser based autofocusing system (Olympus), and an MD-XY30100T-Meta automatically programmable XY stage (SIGMA KOKI). The following were for the multiplexed imaging: an ET430/24x (Chroma

Technology Corp.) excitation filter, an XF2034 (455DRLP) (Omega Optical) dichroic mirror, and FF01-483/32 (Semrock) and ET535-30m (Chroma Technology Corp.) filters for CFP and YFP, respectively. For mCherry, an ET572/35x (Chroma Technology Corp.) excitation filter, 89006-ET-ECFP/EYFP/mCherry (Chroma Technology Corp.) dichroic mirror and an ET632/60m filter (Chroma Technology Corp.) were used.

Images were processed and analyzed with MetaMorph software (Molecular Devices LLC), as described previously (46). Briefly, the FRET efficiency was visualized using the YFP/CFP ratio images shown in the intensity-modulated display mode (IMD), in which 8 colors from red to blue represent the YFP/CFP ratios and 32 grades of color intensity represent the fluorescence intensity of each acceptor fluorophore according to the color scale shown in the respective figure. Melanoma cells expressing artificial GPCR were detected based on the fluorescence of mCherry. To antagonize the EP2 and EP4, 10 μM PF-04418948 (Cayman Chemical Company) and 1 μM ONO-AE3-208 (Cayman Chemical Company) were added to the media.

Intravital imaging by two-photon excitation microscopy

Intravital imaging was performed as previously described with some modifications (47). In brief, mice were anesthetized with 2% isoflurane (FUJIFILM WAKO Pure Chemical Corporation) inhalation (O_2 and air gas ratio was 80:20) and placed in the prone position on an electric heating pad. The body temperature was maintained at 36.5ºC. The skin flap was then placed on a cover-glass.

Living mice were observed with an FV1000MPE-IX-83 inverted microscope (Olympus) equipped with a UPLSAPO 30XS/1.05 numerical aperture (NA) silicon-immersion objective lens (Olympus) and an InSight DeepSee Ultrafast laser (Spectra Physics, Mountain View, CA). The excitation wavelength for GCaMP6s was 930 nm. Fluorescent images were acquired with two different detector channels using the following filters and mirrors: an infrared (IR)-cut filter, BA685RIF-3 (Olympus), two dichroic mirrors, DM505 and DM570 (Olympus), and two

emission filters, FF02-472/30-32 (Semrock, Rochester, NY) for the second harmonic generation (SHG) and BA495-540 HQ (Olympus) for the GCaMP6s. The microscope was equipped with a two-channel GaAsP detector unit and two multialkali detectors. FLUOVIEW software version 4.1a (Olympus) was used to control the microscope and to acquire images, which were saved in the multilayer 16-bit tagged image file format. Images were acquired every 1, 3, and 60 seconds at a scan speed of 2 μs/pixel. Acquired images were processed and analyzed with Metamorph software (Molecular Devices LLC). The dynamics of intracellular Ca^{2+} concentration was analyzed as described above (Time-lapse imaging by wide-field microscopy under *in vitro* conditions). To obtain the proportion of cells experienced Ca^{2+} transients, a fluorescent intensity ratio image depicting the ratio of the maximum intensity projection to the minimum intensity projection over 10 minutes was prepared to represent the fold increase in GCaMP intensity. The ratio images were presented in the intensity-modulated display mode (IMD), with 8 colors from red to blue representing the fold increase in GCaMP intensity and 32 grades of color intensity representing the fluorescence intensity according to the color scale shown in the respective figure. Cells with Ca^{2+} transients were extracted as cells with a high ratio of fluorescence intensity. The proportion of Ca^{2+} transient-positive cells was calculated as the proportion of pixel areas whose fluorescence intensity increased at least 4.5-fold.

***In vivo* cell depletion**

To deplete NK cells, 20 μg anti-asialo GM1 was administered i.p. at day -1 and day 0. To deplete neutrophils, 200 μg anti-Ly6G (1A8) was administered i.p. every other day from one day before tumor implantation (day -1, day 1, and day 3). To deplete macrophages, 100 μl of clodronate liposome was administered i.p. at day -3 and day -1. To deplete platelets, 100 μg anti-CD42b (GPIbα) (R300) was administered i.v. at day 0 and i.p. at day 1.

Bioluminescence imaging

Mice bearing tumors were anesthetized with 2% isoflurane (FUJIFILM WAKO Pure Chemical Corporation) inhalation (O_2 and air gas ratio was over 95%) and placed on a custom-made heating plate in the supine position. Immediately after the administration (i.p.) of 100 µl of 5 mM AkaLumine-HCl, bioluminescent images were acquired using an MIIS system (Molecular Devices Japan) equipped with an iXon Ultra EMCCD camera (Oxford Instruments, Belfast, UK) and a lens (MDJ-G25F095, φ16 mm, F: 0.95, TOKYO PARTS CENTER, Saitama, Japan). Images were acquired under the following conditions: binning, 4; EM gain, 0. Acquisition of bioluminescent images was repeated every 1 minute. The maximum bioluminescent intensity during the imaging was adopted in each mouse. Image acquisition and analysis were carried out with MetaMorph software.

Statistical analysis

Graphing and statistical analysis were performed with GraphPad Prism Software (GraphPad Software, La Jolla, CA). The *p* values were assessed by unpaired Student's two-sample *t*-test.

Results

The GqPCR signaling pathway triggers Ca^{2+} transients in melanoma cells to generate PGE_2 *in vivo*

How can we monitor the secretion of PGE_2? The rate-limiting step in PGE_2 secretion is Ca^{2+}-induced activation of cytosolic phospholipase A2 (cPLA2) (14,48). Therefore, we reasoned that Ca^{2+} transients might be used as a surrogate marker for PGE_2 secretion. To investigate this possibility, we first visualized PGE_2 secretion from $Braf^{V600E}$ melanoma cells by artificially increasing intracellular Ca^{2+} concentrations using the Designer Receptors Exclusively Activated by Designer Drug (DREADD) method (32,49). $Braf^{V600E}$ melanoma cells expressing a Gq-coupled artificial GPCR were stimulated with the agonist clozapine-*N*-oxide (CNO) to elevate the cytoplasmic Ca^{2+} concentration. PGE_2 secretion was monitored by using Madin-Darby canine kidney (MDCK) cells expressing AKAR3EV, a Förster resonance energy transfer (FRET)-based biosensor for PKA (29,30). Secreted PGE_2 will bind to Gs-coupled EP2 and EP4 on the MDCK cells, culminating in PKA activation. As anticipated, CNO induced PKA activation in MDCK cells surrounding the $Braf^{V600E}$ melanoma cells 30 seconds after CNO administration, and the activation ceased within 4 minutes (Figure 1A; Video 1). Pretreatment with inhibitors against EP2 and EP4, PF-04418948 and ONO-AE3-208, respectively, abolished the CNO-induced PKA activation (Figure 1A; Video 1). These results provided the basis for the use of Ca^{2+} transients as a surrogate marker of PGE_2 secretion from $Braf^{V600E}$ melanoma cells.

The Ca^{2+} transients were monitored in $Braf^{V600E}$ melanoma cells expressing a genetically encoded calcium sensor, GCaMP6s (27). Three to five days after subcutaneous implantation, we observed Ca^{2+} transients in the melanoma cells under a two-photon excitation microscope (Figure 1B, 1C; Video 2). When the threshold was set to a 4.5-fold increase in the fluorescence intensity of GCaMP6s, Ca^{2+} transients were observed in 5.3±1.9% of melanoma cells during a 10-minute observation period (data are from 20 mice). In stark contrast to the melanoma cells *in*

vivo, Ca^{2+} transients were rarely observed *in vitro* (Figure 1C; Video 2). These observations suggest that Ca^{2+} transients are induced by ligand(s) supplied from the tumor microenvironment.

There are three major classes of cell surface receptors that trigger Ca^{2+} transients: Gq protein-coupled receptors (GqPCR), calcium channels (CC), and transmembrane receptors directly or indirectly associated with tyrosine kinase (TK) activity (Figure 1D). The contribution of these pathways was examined by using the Gq inhibitor YM-254890, the L-type calcium channel blocker verapamil hydrochloride, and the TK inhibitor dasatinib. Among them, only the Gq inhibitor significantly suppressed Ca^{2+} transients in melanoma cells (Figure 1D). In line with this result, CRISPR/Cas9-mediated gene knockout of *Gnaq*, which encodes guanine nucleotide-binding protein G(q) subunit alpha, abolished Ca^{2+} transients (Figure 1E; Video 3). Re-introduction of the *Gnaq* gene into *Gnaq*$^{-/-}$ cells restored the Ca^{2+} transients to a level similar to that of the parental cells (Figure 1E; Video 3). Collectively, these results indicate that the GqPCR signaling pathway is responsible for triggering Ca^{2+} transients in Braf^{V600E} melanoma cells.

The GqPCR signaling pathway is required for PGE_2 secretion and tumor immune evasion

Autocrine binding of PGE_2 to EP2 and EP4 will trigger cAMP production in melanoma cells (50). Therefore, to monitor the PGE_2 secretion *in vivo*, we examined the transcriptional activity of a cAMP response element (cAMP-RE)-driven promoter that contains three cAMP-REs and a minimal promoter (Figure 2A). The transcriptional activity of cAMP-RE was assessed 4 days after implantation of melanoma cells (Figure 2A). As expected, the transcriptional activity of cAMP-RE was markedly suppressed in *Gnaq*$^{-/-}$ as well as *Ptgs1/Ptgs2*$^{-/-}$ melanoma cells (Figure 2B, left). Comparable levels of bioluminescence were obtained among parental, *Gnaq*$^{-/-}$ and *Ptgs1/Ptgs2*$^{-/-}$ melanoma cells when the ubiquitous promoter CAG was used, negating the possibility that the difference in cell growth rate biased the results (Figure 2B, right). Of note, these cells grew at similar rates *in vitro* (Supplementary figure 1A). In agreement with the

decrease of cAMP-RE transcriptional activity, PGE_2 in *Gnaq*$^{-/-}$ tumors was markedly reduced as well as in *Ptgs1/Ptgs2*$^{-/-}$ tumors (Figure 2C). Collectively, these results demonstrate that the GqPCR-Ca^{2+} signaling pathway plays a major role in the high PGE_2 concentration within tumor tissues.

Do GqPCR-mediated Ca^{2+} transients cause immune evasion? As anticipated, *Gnaq*$^{-/-}$ tumors started to regress around 8 days after implantation as *Ptgs1/Ptgs2*$^{-/-}$ tumors did (Figure 2D). Re-expression of *Gnaq* restored the immune evasion of *Gnaq*$^{-/-}$ tumors (Figure 2D). Pharmacological inhibition of Gq or COX also decreased the growth rate of tumors, albeit less efficiently (Figure 2E). We confirmed that the tumor regression was caused by anti-tumor immunity by using immuno-deficient mice as reported previously (7); *Gnaq*$^{-/-}$ melanoma cells were able to grow in NOD/Shi-scid, IL-2RγKO Jic (NOG) mice as efficiently as parental melanoma cells did (Figure 2F). Moreover, the mice that had already rejected *Gnaq*$^{-/-}$ tumors were resistant to the subsequent challenge with the parental $Braf^{V600E}$ melanoma cells, indicating the development of anti-tumor immunity by the preceding challenge with *Gnaq*$^{-/-}$ melanoma cells (Figure 2G). We negated the possibility that Cas9 expression caused tumor immunity by using the cells expressing Cas9 alone (Supplementary figure 1B).

To extend our findings to another mouse strain, we used 4T1 breast cancer cells having a BALB/c background. We were able to recapitulate Ca^{2+} transients *in vivo*, and the recapitulation was suppressed by a Gq inhibitor, YM-254890 (Supplementary figure 2A). Genetic ablation of Gnaq (*Gnaq*$^{-/-}$) in 4T1 breast cancer cells also resulted in a significant suppression of Ca^{2+} transients (Supplementary figure 2A). As was observed in $Braf^{V600E}$ melanoma cells, *Gnaq*$^{-/-}$ 4T1 breast cancer cells also exhibited a T-cell-dependent rejection 10 days after implantation (Supplementary figure 2B). Collectively, these results demonstrated that the GqPCR pathway drives Ca^{2+} transients and thereby causes immune evasion in both $Braf^{V600E}$ melanoma cells with a C57BL/6 background and 4T1 breast cancer cells with a BALB/c background.

TXA_2-TP signaling triggers Ca^{2+} transients for PGE_2 secretion and tumor immune evasion *in vivo*

Which GqPCR ligand causes Ca^{2+} transients in the $Braf^{V600E}$ melanoma cells *in vivo*? During the course of our experiments, we noticed that the COX inhibitor was able to suppress Ca^{2+} transients in melanoma cells (Supplementary figure 3A, 3B). Thus, we focused on the following three GqPCRs, the ligands of which are COX metabolites: the PGE_2 receptor EP1 subtype encoded by *Ptger1* (EP1), thromboxane A_2 receptor encoded by *Tbxa2r* (TP), and prostaglandin $F_2\alpha$ receptor encoded by *Ptgfr* (FP). Among these, genetic ablation of *Tbxa2r*, but not the others, resulted in almost complete suppression of Ca^{2+} transients (Figure 3A) and marked decrease in intra-tumoral PGE_2 (Figure 3B). Accordingly, $Tbxa2r^{-/-}$ tumors started to regress around 8 days after implantation as observed in $Gnaq^{-/-}$ or $Ptgs1/Ptgs2^{-/-}$ tumors (Figure 3C). The effect of TXA_2 on $Braf^{V600E}$ melanoma cells was confirmed by a TXA_2 mimetic I-BOP. As anticipated, I-BOP triggered Ca^{2+} transients under in $Braf^{V600E}$ melanoma cells (Supplementary figure 4). These results clearly identified TXA_2-TP signaling as the primary pathway that dictates Ca^{2+} transients, thereby facilitating PGE_2 secretion and tumor immune evasion.

VEGF receptor signaling is indispensable for TXA_2-mediated PGE_2 secretion

TXA_2 was originally described as being released from platelets, but is now known to be released by a variety of cells, including myeloid-lineage cells and endothelial cells (51,52). This raises a question: Which host cells produce TXA_2 to stimulate melanoma cells? Or do tumor cells themselves secrete TXA_2? Knockout of thromboxane A synthase 1 in melanoma cells ($Tbxas1^{-/-}$) did not have any effect on Ca^{2+} transients, negating the autocrine stimulation of TP (Figure 4A). Next, we attempted to determine the time point at which the tumor cells begin to exhibit Ca^{2+} transients after implantation into the subcutaneous tissue. We found that the proportion of Ca^{2+} transient-positive cells reached its zenith 2 days after implantation, implying the involvement of infiltrating host cells to trigger Ca^{2+} transients in melanoma cells (Figure 4B).

To determine the source of TXA_2, we performed *in vivo* cell depletion, using specific antibodies targeting platelets or neutrophils, clodronate liposome targeting macrophages, and NOG mice. However, none of these conditions suppressed the Ca^{2+} transients in melanoma cells (Supplementary figure 5A, 5B).

To gain an insight into the origin of intra-tumoral TXA_2, we examined contribution of vascular endothelial growth factor (VEGF), which has been implicated in recruitment of myeloid-lineage cells (53,54) and induction of TXA_2 synthesis in vascular endothelial cells (45). We first confirmed that VEGF triggered TXA_2 secretion from human umbilical vein endothelial cells (HUVECs) (Supplementary figure 5C). Because of the short half-life, TXA_2 is typically monitored by measurement of TXB_2. In this study, the concentration of TXB_2 was considered as that of TXA_2. We next examined the effect of a VEGFR inhibitor, motesanib, on TXA_2-TP mediated PGE_2 secretion from melanoma cells. Intravital imaging revealed that Ca^{2+} transients in melanoma cells were robustly suppressed within 30 minutes after i.v. administration of motesanib (Figure 4C; Video 4). Accordingly, intra-tumoral TXA_2 and PGE_2 concentrations were decreased after motesanib administration (Figure 4D). Therefore, these results strongly suggest that VEGF increases intra-tumoral TXA_2 and, thereby, drives melanoma cells to secrete PGE_2. Altogether, we clarified the indispensable role of VEGF receptor signaling in PGE_2 secretion mediated by host cell-derived TXA_2, providing a molecular basis underlying the immunomodulatory effect of anti-VEGF therapies.

Tumor cell-derived COX-1 metabolites are required to induce Ca^{2+} transients and locally promote tumor immune evasion

During the course of our experiments, we noticed that genetic ablation of both COX-1 and COX-2 genes (*Ptgs1/Ptgs2*$^{-/-}$) also decreased the fraction of the Ca^{2+} transient-positive cells (Figure 5A, 5B). Further analysis revealed that genetic ablation of COX-1 (*Ptgs1*$^{-/-}$) alone was sufficient for this inhibition (Figure 5A, 5B). This observation was unexpected, because we

considered PGE_2 secretion as a downstream event of Ca^{2+} transients in tumor cells. COX-1 and COX-2 are considered to be constitutive and inducible enzymes, respectively (55). Therefore, we speculate that tumor cell-derived COX-1 metabolites, probably PGE_2, is required in the early phase of TME establishment to render the TME prone to inducing Ca^{2+} transients in melanoma cells for PGE_2 secretion.

Finally, we examined the possibility that COX metabolites can systemically modulate the TME to induce Ca^{2+} transients by using a bilateral tumor burden model. When GCaMP6s-expressing parental cells were inoculated contralaterally, *Ptgs1/Ptgs2*$^{-/-}$ cells carrying the Ca^{2+} indicator did not show Ca^{2+} transients (Figure 5C). However, when *Ptgs1/Ptgs2*$^{-/-}$ cells were mixed with parental cells without GCaMP6s and inoculated ipsilaterally, the *Ptgs1/Ptgs2*$^{-/-}$ cells exhibited Ca^{2+} transients (Figure 5C). To confirm that the effect of COX metabolites is limited to local melanoma cells, we examined the transcriptional activity of the Ca^{2+}-responsive NFAT promoter (Figure 5D). The transcriptional activity of the NFAT promoter in *Ptgs1/Ptgs2*$^{-/-}$ cells was markedly lower than that of parental cells injected contralaterally (Figure 5D). The NFAT activity in parental cells was also suppressed by daily i.p. injection of a COX inhibitor, flurbiprofen. A similar result was obtained by using *Gnaq*$^{-/-}$ cells (Figure 5D). Further, contralateral inoculation of parental cells did not result in any enhanced growth of *Ptgs1/Ptgs2*$^{-/-}$ cells or *Gnaq*$^{-/-}$ cells (Figure 5IE). Collectively, these results indicate that COX-1 metabolites, probably PGE_2, acts locally to induce Ca^{2+} transients and promote tumor immune evasion.

Discussion

In stark contrast to the plethora of data about the effects of tumor cell-derived PGE_2, little is known about how the secretion of PGE_2 is regulated within the TME. Here, we have provided evidence that VEGF receptor signaling plays a pivotal role in tumor cell-derived PGE_2 secretion mediated by host cell-derived TXA_2, thereby promoting tumor immune evasion (Figure 6). Phenotypes of melanoma cells deficient in *Tbxa2r* or *Gnaq* are mirror images of *Ptgs1/Ptgs2*$^{-/-}$ melanoma cells, which fail to evade immune surveillance (Figure 1-3) (4,7), indicating that TP-mediated Gq signaling dictates PGE_2 secretion, at least in $Braf^{V600E}$ melanoma cells and 4T1 breast cancer cells. TXA_2 has been shown to promote tumor metastasis by activating platelets and coagulation cascades (16). In addition, a phenome-wide association study has revealed an association between a single nucleotide polymorphism in the *TBXA2R* gene and multiple secondary malignancies (56). Our observation adds a new function, evasion of tumor immunity, to TXA_2.

VEGF, which was initially identified as a vascular permeability factor (57), is now recognized as one of the most potent promoters of various aspects of tumorigenesis, including angiogenesis, invasiveness, metastasis, and recurrence (58). Moreover, previous studies have also demonstrated that anti-VEGF therapy activates anti-tumor immunity in animal models (59-61). In line with these animal experiments, the VEGF neutralizing antibody bevacizumab increases both the number and maturation of dendritic cells (DCs) in patients with metastatic non-small cell lung carcinoma (NSCLC) (62). The augmentation of intra-tumoral T-cell infiltration by bevacizumab treatment in combination with anti-PD-L1 checkpoint inhibition has also been reported in patients with metastatic renal cell carcinoma (RCC) (63). Several clinical trials in melanoma, RCC, NSCLC, and hepatocellular carcinoma have successfully evaluated the combination of immune checkpoint inhibitors (ICIs) with VEGF/VEGFR blockade (64). Indeed, ICIs in combination with VEGFR inhibitors have become a new standard of care in treatment-naïve patients with advanced RCC (65). The new pathway revealed in this study—i.e., VEGF-

516 mediated PGE_2 secretion from tumor cells (Figure 4)— provides a molecular basis underlying
517 the effect of anti-VEGF therapy on the augmentation of tumor immunity.
518 How does VEGF induce TXA_2 within tumor tissues? Upon motesanib administration, it took
519 only 20 minutes until the suppression of Ca^{2+} transients (Figure 4C). Therefore, we can speculate
520 that VEGF drives TXA_2 secretion from host cells through the activation of cPLA2 without gene
521 expression change (66). Alternatively, VEGF may cause leakage of intravascular TXA_2 by
522 maintaining high vascular permeability in the tumor tissue. Our previous study revealed that anti-
523 VEGFR reduces vascular permeability through the activation of PKA activity in endothelial cells
524 (47). The time-course of the PKA activation was similar to that of suppression of Ca^{2+} transients
525 in the current study, suggesting that TXA_2 may be derived from blood. Further studies are
526 needed to clarify the precise role of VEGFR signaling in increasing intra-tumoral TXA_2
527 concentration, promoting PGE_2 secretion and tumor immune evasion.
528 Intravital imaging of mice is one of the cutting-edge techniques to untangle the complex
529 intercellular communications within the TME, as it provides information on cell dynamics at the
530 single-cell level (19,67). The TME contains stromal cells and immune cells that shape tumor
531 development and impact the response to anti-tumor therapy (67,68). Modulation of the TME by
532 tumor cell-intrinsic oncogenic signaling is increasingly recognized to have key roles in initiating
533 and supporting tumorigenesis both in solid tumors and hematological malignancies (69,70).
534 Importantly, such cell-to-cell communication cannot be recapitulated in most tissue culture
535 systems. In fact, we rarely observe PGE_2 secretion from melanoma cells under *in vitro* conditions
536 in the absence of stimulation (Figure 1C). Only intravital imaging of tumor cells has enabled us
537 to uncover PGE_2 secretion from a small fraction of tumor cells (Figure 1C). This raises a
538 question: Why don't all tumor cells exhibit Ca^{2+} transients? One possibility is the difference in
539 responsiveness among tumor cells. In fact, even under *in vitro* conditions, we observed that only
540 fraction of cells exhibited Ca^{2+} transients upon the stimulation with TP agonist, I-BOP,
541 suggesting the heterogeneity in responsiveness (Supplementary figure 4). However, there might

be difference between *in vivo* and *in vitro* conditions. Another possibility is that tumor cells in close proximity to TXA_2-secreting cells may exhibit Ca^{2+} transients. Further analysis with high resolution intravital imaging of both tumor cells and host cells in combination with techniques to visualize the activation status of host cells would lead to an answer.

One of the most surprising results of our study was that COX ablation, especially COX-1 ablation, abolished Ca^{2+} transients in melanoma cells (Figure 5A, 5B). Although COX-1 has received less attention compared to COX-2, its expression indeed increases in several human cancers, and a pathogenetic role of COX-1 has emerged from several experimental models (3,71). Considering the results of genetic ablation in TXA_2 synthase (Figure 4A), our data support the notion that PGE_2 secreted from melanoma cells promotes PGE_2 secretion via enhancement of the TXA_2 secretion from host cells (Figure 6). This kind of positive feedback for PGE_2 secretion has rarely been observed but is still suggested to exist under physiological and pathological conditions, including tumorigenesis, focusing on the expression level of proteins regulating PGE_2 synthesis (72-75). Our current study stands out among other related investigations in that we focused exclusively on the intercellular communication circuits based on the signal transduction through GqPCR.

Ever since treatment with nonsteroidal anti-inflammatory drugs (NSAIDs) was showed to elicit an anti-tumor effect in mouse models and human patients, investigators have focused on the importance of prostanoids, especially PGE_2 (3). However, NSAIDs are not prescribed to treat or prevent cancer in clinical settings due to the severe side effects associated with long-term administration of NSAIDS, which include gastrointestinal, renal, and cardiovascular disorders (71,76,78,80). Currently, NSAIDs are used as the synonym of COX inhibitors. Our study shows that other gene products associated with the arachidonic acid cascade should also provide clues to the future development of anti-cancer drugs. In this study, we have shown that TXA_2 released from host cells stimulates PGE_2 secretion and tumor immune evasion. VEGF receptor signaling plays the indispensable role in this intercellular communication circuits. The TXA_2-TP signaling

pathway and/or VEGR receptor signaling pathway would be promising targetable component of the PGE_2 secretion machinery, and thus could give rise to novel strategies for the prevention and/or treatment of multiple types of malignancies, especially in combination with immunomodulatory agents.

Supplemental information

Supplemental information including five figures and four videos can be found with this article online.

Acknowledgements

We are grateful to Dean Thumkeo for technical suggestions on the quantification of PGE_2, the members of the Matsuda Laboratory for their helpful input, particularly K. Hirano, K. Takakura, A. Kawagishi and Y. Takeshita, who provided technical assistance, and to the Medical Research Support Center of Kyoto University for DNA sequence analysis. This work was supported by the Kyoto University Live Imaging Center. Financial support was provided by JSPS KAKENHI grant nos. 16J09066 (to Y.K.), 19K23915 (to Y.K.), 20K17400 (to Y.K.), 20J01623 (to Y.K.), 18K07066 (to K.T.), 15H05949 (to M.M.), and 16H06280 (to M.M.) and JST CREST no. JPMJCR1654 (to M.M.).

Author contributions

Conceptualization, Y.K., K.T., and M.M.; Methodology, Y.K., H.I., T.W., C.O., S.T., Y.H., T.K., and M.M.; Validation, Y.K., K.T. and M.M.; Formal Analysis, Y.K., K.T., and M.M.; Investigation, Y.K., H.I., T.W., and K.T.; Data Curation, Y.K., and M.M.; Resources, Y.K., C.O., S.T., K.T., and M.M.; Writing – Original Draft, Y.K.; Writing – Review & Editing, S.T., Y.H., Y.M., A.T-K., T.,K., and M.M.; Supervision, T.K. and M.M.; Project Administration, T.K. and M.M.; Funding Acquisition, Y.K., T.K., and M.M.

Declaration of Interests

The authors declare no competing interests.

References

1. Dannenberg AJ, Subbaramaiah K. Targeting cyclooxygenase-2 in human neoplasia: Rationale and promise. Cancer Cell **2003**;4:431-6
2. Kalinski P. Regulation of Immune Responses by Prostaglandin E2. The Journal of Immunology **2012**;188:21-8
3. Wang D, DuBois RN. Eicosanoids and cancer. Nature Reviews Cancer **2010**;10:181-93
4. Böttcher JP, Bonavita E, Chakravarty P, Blees H, Cabeza-Cabrerizo M, Sammicheli S, *et al.* NK Cells Stimulate Recruitment of cDC1 into the Tumor Microenvironment Promoting Cancer Immune Control. Cell **2018**;172:1022-37.e14
5. Chen JH, Perry CJ, Tsui Y-C, Staron MM, Parish IA, Dominguez CX, *et al.* Prostaglandin E2 and programmed cell death 1 signaling coordinately impair CTL function and survival during chronic viral infection. Nature Medicine **2015**;21:327-34
6. Pietra G, Manzini C, Rivara S, Vitale M, Cantoni C, Petretto A, *et al.* Melanoma Cells Inhibit Natural Killer Cell Function by Modulating the Expression of Activating Receptors and Cytolytic Activity. Cancer Research **2012**;72:1407
7. Zelenay S, van der Veen Annemarthe G, Böttcher Jan P, Snelgrove Kathryn J, Rogers N, Acton Sophie E, *et al.* Cyclooxygenase-Dependent Tumor Growth through Evasion of Immunity. Cell **2015**;162:1257-70
8. Su Y, Jackson EK, Gorelik E. Receptor desensitization and blockade of the suppressive effects of prostaglandin E2 and adenosine on the cytotoxic activity of human melanoma-infiltrating T lymphocytes. Cancer Immunology, Immunotherapy **2011**;60:111-22
9. Greenhough A, Smartt HJM, Moore AE, Roberts HR, Williams AC, Paraskeva C, *et al.* The COX-2/PGE2 pathway: key roles in the hallmarks of cancer and adaptation to the tumour microenvironment. Carcinogenesis **2009**;30:377-86
10. Park JY, Pillinger MH, Abramson SB. Prostaglandin E2 synthesis and secretion: The role of PGE2 synthases. Clinical Immunology **2006**;119:229-40
11. Sugimoto Y, Narumiya S. Prostaglandin E receptors. Journal of Biological Chemistry **2007**;282:11613-7
12. Kawahara K, Hohjoh H, Inazumi T, Tsuchiya S, Sugimoto Y. Prostaglandin E2-induced inflammation: Relevance of prostaglandin E receptors. Biochimica et Biophysica Acta (BBA) - Molecular and Cell Biology of Lipids **2015**;1851:414-21
13. Kita Y, Shindou H, Shimizu T. Cytosolic phospholipase A2 and lysophospholipid acyltransferases. Biochimica et biophysica acta Molecular and cell biology of lipids **2019**;1864:838-45
14. Gijón MA, Leslie CC. Regulation of arachidonic acid release and cytosolic Phospholipase A2 activation. Journal of Leukocyte Biology **1999**;65:330-6
15. Félétou M, Verbeuren TJ, Vanhoutte PM. Endothelium-dependent contractions in SHR: a tale of prostanoid TP and IP receptors. **2009**;156:563-74
16. Francisco BJ, Palumbo JS. New insights into cancer's exploitation of platelets. Journal of Thrombosis and Haemostasis **2019**;17:2000-3
17. Friedl P, Locker J, Sahai E, Segall JE. Classifying collective cancer cell invasion. Nature Cell Biology **2012**;14:777-83
18. Germain RN, Robey EA, Cahalan MD. A decade of imaging cellular motility and interaction dynamics in the immune system. Science **2012**;336:1676-81
19. Miller MA, Weissleder R. Imaging of anticancer drug action in single cells. Nat Rev Cancer **2017**;17:399-414
20. Nobis M, Warren SC, Lucas MC, Murphy KJ, Herrmann D, Timpson P. Molecular mobility and activity in an intravital imaging setting – implications for cancer progression and targeting. Journal of Cell Science **2018**;131:jcs206995
21. Thibaut R, Bost P, Milo I, Cazaux M, Lemaître F, Garcia Z, *et al.* Bystander IFN-γ activity promotes widespread and sustained cytokine signaling altering the tumor microenvironment. Nature Cancer **2020**;1:302-14

22. Hirata E, Maria, Viros A, Hooper S, Spencer-Dene B, Matsuda M, *et al.* Intravital Imaging Reveals How BRAF Inhibition Generates Drug-Tolerant Microenvironments with High Integrin β1/FAK Signaling. Cancer Cell **2015**;27:574-88
23. Vennin C, Chin VT, Warren SC, Lucas MC, Herrmann D, Magenau A, *et al.* Transient tissue priming via ROCK inhibition uncouples pancreatic cancer progression, sensitivity to chemotherapy, and metastasis. Science Translational Medicine **2017**;9:eaai8504
24. Terai K, Imanishi A, Li C, Matsuda M. Two decades of genetically encoded biosensors based on Förster resonance energy transfer. Cell Structure and Function **2019**;advpub
25. Greenwald EC, Mehta S, Zhang J. Genetically Encoded Fluorescent Biosensors Illuminate the Spatiotemporal Regulation of Signaling Networks. Chemical Reviews **2018**
26. Iwano S, Sugiyama M, Hama H, Watakabe A, Hasegawa N, Kuchimaru T, *et al.* Single-cell bioluminescence imaging of deep tissue in freely moving animals. Science **2018**;359:935
27. Chen T-W, Wardill TJ, Sun Y, Pulver SR, Renninger SL, Baohan A, *et al.* Ultrasensitive fluorescent proteins for imaging neuronal activity. Nature **2013**;499:295-300
28. Shaner NC, Campbell RE, Steinbach PA, Giepmans BNG, Palmer AE, Tsien RY. Improved monomeric red, orange and yellow fluorescent proteins derived from Discosoma sp. red fluorescent protein. Nature Biotechnology **2004**;22:1567-72
29. Komatsu N, Aoki K, Yamada M, Yukinaga H, Fujita Y, Kamioka Y, *et al.* Development of an optimized backbone of FRET biosensors for kinases and GTPases. Molecular Biology of the Cell **2011**;22:4647-56
30. Watabe T, Terai K, Sumiyama K, Matsuda M. Booster, a Red-Shifted Genetically Encoded Förster Resonance Energy Transfer (FRET) Biosensor Compatible with Cyan Fluorescent Protein/Yellow Fluorescent Protein-Based FRET Biosensors and Blue Light-Responsive Optogenetic Tools. ACS Sens **2020**;5:719-30
31. Goedhart J, von Stetten D, Noirclerc-Savoye M, Lelimousin M, Joosen L, Hink MA, *et al.* Structure-guided evolution of cyan fluorescent proteins towards a quantum yield of 93%. Nature Communications **2012**;3:751
32. Goto A, Nakahara I, Yamaguchi T, Kamioka Y, Sumiyama K, Matsuda M, *et al.* Circuit-dependent striatal PKA and ERK signaling underlies rapid behavioral shift in mating reaction of male mice. Proceedings of the National Academy of Sciences **2015**;112:6718-23
33. Miyoshi H, Blömer U, Takahashi M, Gage FH, Verma IM. Development of a Self-Inactivating Lentivirus Vector. Journal of Virology **1998**;72:8150
34. Yusa K, Rad R, Takeda J, Bradley A. Generation of transgene-free induced pluripotent mouse stem cells by the piggyBac transposon. Nature methods **2009**;6:363-9
35. Kim JH, Lee S-R, Li L-H, Park H-J, Park J-H, Lee KY, *et al.* High cleavage efficiency of a 2A peptide derived from porcine teschovirus-1 in human cell lines, zebrafish and mice. PloS one **2011**;6:e18556-e
36. Komatsu N, Terai K, Imanishi A, Kamioka Y, Sumiyama K, Jin T, *et al.* A platform of BRET-FRET hybrid biosensors for optogenetics, chemical screening, and in vivo imaging. Scientific Reports **2018**;8:8984
37. Durand DB, Shaw JP, Bush MR, Replogle RE, Belagaje R, Crabtree GR. Characterization of antigen receptor response elements within the interleukin-2 enhancer. Molecular and Cellular Biology **1988**;8:1715
38. Granelli-Piperno A, McHugh P. Characterization of a protein that regulates the DNA-binding activity of NF-AT, the nuclear factor of activated T cells. Proceedings of the National Academy of Sciences of the United States of America **1991**;88:11431-4
39. Spengler D, Rupprecht R, Van LP, Holsboer F. Identification and characterization of a 3',5'-cyclic adenosine monophosphate-responsive element in the human corticotropin-releasing hormone gene promoter. Molecular Endocrinology **1992**;6:1931-41
40. Kawakami K, Takeda H, Kawakami N, Kobayashi M, Matsuda N, Mishina M. A Transposon-Mediated Gene Trap Approach Identifies Developmentally Regulated Genes in Zebrafish. Developmental Cell **2004**;7:133-44

41. Kuchimaru T, Iwano S, Kiyama M, Mitsumata S, Kadonosono T, Niwa H, *et al.* A luciferin analogue generating near-infrared bioluminescence achieves highly sensitive deep-tissue imaging. Nature Communications **2016**;7:11856
42. Dhomen N, Reis-Filho JS, da Rocha Dias S, Hayward R, Savage K, Delmas V, *et al.* Oncogenic Braf Induces Melanocyte Senescence and Melanoma in Mice. Cancer Cell **2009**;15:294-303
43. Naito Y, Hino K, Bono H, Ui-Tei K. CRISPRdirect: software for designing CRISPR/Cas guide RNA with reduced off-target sites. Bioinformatics **2014**;31:1120-3
44. Nie X, Kitaoka S, Shinohara M, Kakizuka A, Narumiya S, Furuyashiki T. Roles of Toll-like receptor 2/4, monoacylglycerol lipase, and cyclooxygenase in social defeat stress-induced prostaglandin E2 synthesis in the brain and their behavioral relevance. Scientific Reports **2019**;9:17548
45. Nie D, Lamberti M, Zacharek A, Li L, Szekeres K, Tang K, *et al.* Thromboxane A2 Regulation of Endothelial Cell Migration, Angiogenesis, and Tumor Metastasis. Biochemical and Biophysical Research Communications **2000**;267:245-51
46. Konishi Y, Terai K, Furuta Y, Kiyonari H, Abe T, Ueda Y, *et al.* Live-Cell FRET Imaging Reveals a Role of Extracellular Signal-Regulated Kinase Activity Dynamics in Thymocyte Motility. iScience **2018**;10:98-113
47. Yamauchi F, Kamioka Y, Yano T, Matsuda M. In Vivo FRET Imaging of Tumor Endothelial Cells Highlights a Role of Low PKA Activity in Vascular Hyperpermeability. Cancer Research **2016**;76:5266-76
48. Hirabayashi T, Kume K, Hirose K, Yokomizo T, Iino M, Itoh H, *et al.* Critical Duration of Intracellular Ca2+ Response Required for Continuous Translocation and Activation of Cytosolic Phospholipase A2. **1999**;274:5163-9
49. Armbruster BN, Li X, Pausch MH, Herlitze S, Roth BL. Evolving the lock to fit the key to create a family of G protein-coupled receptors potently activated by an inert ligand. Proceedings of the National Academy of Sciences **2007**;104:5163-8
50. O'Callaghan G, Houston A. Prostaglandin E2 and the EP receptors in malignancy: possible therapeutic targets? British journal of pharmacology **2015**;172:5239-50
51. Smyth EM. Thromboxane and the thromboxane receptor in cardiovascular disease. Clin Lipidol **2010**;5:209-19
52. Sellers MM, Stallone JN. Sympathy for the devil: the role of thromboxane in the regulation of vascular tone and blood pressure. American Journal of Physiology-Heart and Circulatory Physiology **2008**;294:H1978-H86
53. Sawano A, Iwai S, Sakurai Y, Ito M, Shitara K, Nakahata T, *et al.* Flt-1, vascular endothelial growth factor receptor 1, is a novel cell surface marker for the lineage of monocyte-macrophages in humans. Blood **2001**;97:785-91
54. Barleon B, Sozzani S, Zhou D, Weich HA, Mantovani A, Marmé D. Migration of human monocytes in response to vascular endothelial growth factor (VEGF) is mediated via the VEGF receptor flt-1. Blood **1996**;87:3336-43
55. Smith WL, DeWitt DL, Garavito RM. Cyclooxygenases: Structural, Cellular, and Molecular Biology. Annual Review of Biochemistry **2000**;69:145-82
56. Pulley JM, Jerome RN, Ogletree ML, Bernard GR, Lavieri RR, Zaleski NM, *et al.* Motivation for Launching a Cancer Metastasis Inhibition (CMI) Program. Target Oncol **2018**;13:61-8
57. Senger DR, Galli SJ, Dvorak AM, Perruzzi CA, Harvey VS, Dvorak HF. Tumor cells secrete a vascular permeability factor that promotes accumulation of ascites fluid. Science **1983**;219:983-5
58. Apte RS, Chen DS, Ferrara N. VEGF in Signaling and Disease: Beyond Discovery and Development. Cell **2019**;176:1248-64
59. Allen E, Jabouille A, Rivera LB, Lodewijckx I, Missiaen R, Steri V, *et al.* Combined antiangiogenic and anti–PD-L1 therapy stimulates tumor immunity through HEV formation. Science Translational Medicine **2017**;9:eaak9679
60. Schmittnaegel M, Rigamonti N, Kadioglu E, Cassará A, Wyser Rmili C, Kiialainen A, *et al.* Dual angiopoietin-2 and VEGFA inhibition elicits antitumor immunity that is enhanced by PD-1 checkpoint blockade. Science Translational Medicine **2017**;9:eaak9670

61. Shrimali RK, Yu Z, Theoret MR, Chinnasamy D, Restifo NP, Rosenberg SA. Antiangiogenic Agents Can Increase Lymphocyte Infiltration into Tumor and Enhance the Effectiveness of Adoptive Immunotherapy of Cancer. Cancer Research **2010**;70:6171-80
62. Martino E, Misso G, Pastina P, Costantini S, Vanni F, Gandolfo C, *et al.* Immune-modulating effects of bevacizumab in metastatic non-small-cell lung cancer patients. **2016**;2:16025
63. Wallin JJ, Bendell JC, Funke R, Sznol M, Korski K, Jones S, *et al.* Atezolizumab in combination with bevacizumab enhances antigen-specific T-cell migration in metastatic renal cell carcinoma. Nature Communications **2016**;7:12624
64. Ntellas P, Mavroeidis L, Gkoura S, Gazouli I, Amylidi A-L, Papadaki A, *et al.* Old Player-New Tricks: Non Angiogenic Effects of the VEGF/VEGFR Pathway in Cancer. Cancers (Basel) **2020**;12:3145
65. Hirsch L, Flippot R, Escudier B, Albiges L. Immunomodulatory Roles of VEGF Pathway Inhibitors in Renal Cell Carcinoma. Drugs **2020**;80:1169-81
66. Koch S, Claesson-Welsh L. Signal transduction by vascular endothelial growth factor receptors. Cold Spring Harb Perspect Med **2012**;2:a006502-a
67. Binnewies M, Roberts EW, Kersten K, Chan V, Fearon DF, Merad M, *et al.* Understanding the tumor immune microenvironment (TIME) for effective therapy. Nature Medicine **2018**;24:541-50
68. Nguyen KB, Spranger S. Modulation of the immune microenvironment by tumor-intrinsic oncogenic signaling. The Journal of Cell Biology **2020**;219
69. Ghobrial IM, Detappe A, Anderson KC, Steensma DP. The bone-marrow niche in MDS and MGUS: implications for AML and MM. Nature Reviews Clinical Oncology **2018**;15:219
70. Spranger S, Gajewski TF. Impact of oncogenic pathways on evasion of antitumour immune responses. Nature Reviews Cancer **2018**;18:139-47
71. Pannunzio A, Coluccia M. Cyclooxygenase-1 (COX-1) and COX-1 Inhibitors in Cancer: A Review of Oncology and Medicinal Chemistry Literature. Pharmaceuticals (Basel) **2018**;11:101
72. Attar E, Bulun SE. Aromatase and other steroidogenic genes in endometriosis: translational aspects. Hum Reprod Update **2006**;12:49-56
73. Obermajer N, Muthuswamy R, Lesnock J, Edwards RP, Kalinski P. Positive feedback between PGE2 and COX2 redirects the differentiation of human dendritic cells toward stable myeloid-derived suppressor cells. Blood **2011**;118:5498-505
74. Yoshida K, Fujino H, Otake S, Seira N, Regan JW, Murayama T. Induction of cyclooxygenase-2 expression by prostaglandin E2 stimulation of the prostanoid EP4 receptor via coupling to Gαi and transactivation of the epidermal growth factor receptor in HCA-7 human colon cancer cells. European Journal of Pharmacology **2013**;718:408-17
75. Tamura K, Naraba H, Hara T, Nakamura K, Yoshie M, Kogo H, *et al.* A positive feedback loop between progesterone and microsomal prostaglandin E synthase-1-mediated PGE2 promotes production of both in mouse granulosa cells. Prostaglandins & Other Lipid Mediators **2016**;123:56-62
76. Kobayashi K, Omori K, Murata T. Role of prostaglandins in tumor microenvironment. Cancer and Metastasis Reviews **2018**;37:347-54

Figure legends

Figure 1. The GqPCR signaling pathway triggers Ca^{2+} transients in melanoma cells to generate PGE_2 *in vivo*

(A) Melanoma cells expressing the DREADD hM_3 (artificial GqPCR) were stimulated by 1 μM CNO treatment. A representative melanoma cell is shown in white and indicated by a white arrow. Secretion of PGE_2 was monitored by changes of PKA activity in surrounding MDCK cells (shown in green), which were visualized by a PKA biosensor. The time course of PKA activity in surrounding MDCK cells after CNO treatment was visualized as ratio images shown in the IMD mode. Pretreatment with inhibitors against EP2 (10 μM PF-04418948) and EP4 (1 μM ONO-AE3-208) abolished the activation of PKA. (B) Melanoma cells expressing GCaMP6s were observed in living mice 3 to 5 days after subcutaneous implantation. (C) Parental melanoma cells expressing GCaMP6s were imaged under *in vivo* conditions and *in vitro* culture conditions. Each image represents the maximum intensity projection for 10 minutes. The fluorescence time course of GCaMP6s in each cell was quantified as the fold increase in fluorescence intensity at each time point to fluorescence intensity of minimum intensity projection over 10 minutes. The fluorescence intensity was measured by averaging all pixels within the region of interest (ROI) in each cell. (D) Gq protein-coupled receptors (GqPCRs), calcium channels (CCs), and transmembrane receptors directly or indirectly associated with tyrosine kinase activity (TK), such as Src family, Abl family, and ErbB family, etc., are three groups of major membrane proteins that trigger calcium transients. The dynamics of intracellular Ca^{2+} concentration *in vivo* was visualized in parental melanoma cells treated with a Gq inhibitor (i.v., 0.6 mg/kg YM-254890). Each image represents the fold increase in fluorescence intensity over 10 minutes before and 20 minutes after drug treatment. The proportion of Ca^{2+} transient-positive cells was quantified before and 20 minutes after treatment with a Gq inhibitor, CC blocker (i.p., 1 mg/kg verapamil hydrochloride), and TK inhibitor (i.v., 10 mg/kg dasatinib). Each line represents an individual mouse experiment. (E) The dynamics of intracellular Ca^{2+}

concentration *in vivo* was visualized in parental melanoma, *Gnaq*$^{-/-}$ melanoma, and *Gnaq*$^{-/-}$ melanoma introduced with Gnaq (*Gnaq*$^{-/-}$ + Gnaq). Each image represents the fold increase in fluorescence intensity over 10 minutes. Each dot represents the proportion of Ca^{2+} transient-positive cells in an individual mouse (data from 3 or 4 mice per group). All the p-values were assessed by unpaired Student's two-sample *t*-test.

Figure 2. The GqPCR signaling pathway is required for PGE_2 secretion and tumor immune evasion

(A) The transcriptional activity of cAMP-RE was assessed by an Akaluc luciferase-based reporter assay 4 days after implantation. Representative merged images of the bright field and the bioluminescence images of mice implanted with parental, *Ptgs1*/*Ptgs2*$^{-/-}$, and *Gnaq*$^{-/-}$ melanoma cells are shown. (B) Each dot represents the bioluminescence intensity of an individual tumor. The expression of the reporter gene was regulated by a cAMP-RE-driven promoter or CAG promoter. (C) Concentration of PGE_2 in lysates from total tumors 4 days after implantation. C57BL/6NCrSlc mice were implanted with parental, *Gnaq*$^{-/-}$, and *Ptgs1*/*Ptgs2*$^{-/-}$ melanoma cells. Each dot represents an independent tumor. D) C57BL/6NCrSlc mice were inoculated with 2 x10^5 parental or *Gnaq*$^{-/-}$cells, parental or *Ptgs1/Ptgs2*$^{-/-}$cells, and *Gnaq*$^{-/-}$ cells or *Gnaq*$^{-/-}$ melanoma cells introduced with Gnaq (*Gnaq*$^{-/-}$ + Gnaq) (E) C57BL/6NCrSlc mice inoculated with 2 x10^5 parental cells were treated with or without Gq inhibitor (s.c., 0.5 mg/kg YM-254890, daily from day 0) or with or without COX inhibitor (i.p., 25 mg/kg flurbiprofen axetil, daily from day 0). Each line represents the growth of an individual tumor inoculated in mice. Data represent one of two independent experiments with 3 or 4 mice per group. (F) NOD/Shi-scid, IL-2RγKO Jic (NOG) mice were inoculated with 2 x10^5 parental or *Gnaq*$^{-/-}$ melanoma cells. Each line represents the growth of an individual tumor inoculated in mice. Data represent one of two independent experiments with 3 or 4 mice per group. (G) Parental melanoma cells were implanted into naïve C57BL/6NCrSlc mice or mice that previously rejected

Gnaq$^{-/-}$ cells (pre-inoculated). Each line represents the growth of an individual tumor inoculated in mice. Data represent one of two independent experiments with 4 mice per group. All the p-values were assessed by unpaired Student's two-sample *t*-test.

Figure 3. TXA_2-TP triggers Ca^{2+} transients for PGE_2 secretion and tumor immune evasion *in vivo*

(A) The dynamics of intracellular Ca^{2+} concentration *in vivo* was visualized in parental, *Tbxa2r*$^{-/-}$, *Ptger1*$^{-/-}$, and *Ptgfr*$^{-/-}$ melanoma cells. Each image represents the fold increase in fluorescence intensity over 10 minutes. Each dot represents the proportion of Ca^{2+} transient-positive cells in an individual mouse (data from 3 or 4 mice per group). (B) Concentration of PGE_2 in lysates from total tumors 4 days after implantation. C57BL/6NCrSlc mice were implanted with parental and *Tbxa2r*$^{-/-}$ melanoma cells. Each dot represents an independent tumor. (C) C57BL/6NCrSlc mice were inoculated with 2 x10^5 parental or *Tbxa2r*$^{-/-}$ melanoma cells. Each line represents the growth of an individual tumor inoculated in mice. Data represent one of two independent experiments with 4 to 5 mice per group. All the p-values were assessed by unpaired Student's two-sample *t*-test.

Figure 4. VEGF receptor signaling is indispensable for TXA_2- mediated PGE_2 secretion

(A-C) The dynamics of intracellular Ca^{2+} concentration *in vivo* was visualized (A) in parental melanoma and *Tbxas1*$^{-/-}$ melanoma cells, (B) parental melanoma cells 1 day (18–24 hours), 2 days (46–52 hours), and 3 days (72–85 hours) after implantation, and (C) parental melanoma cells before treatment, 20 minutes, and 30 minutes after treatment with VEGFR inhibitor (i.v., 75 mg/kg motesanib). Each image represents the fold increase in fluorescence intensity over 10 minutes. Each dot in the graph represents the proportion of Ca^{2+} transient-positive cells in an individual mouse (data from 3 to 5 mice per group). (D) Concentration of TXB_2 and PGE_2 in lysates from parental melanoma tumors 4 days after implantation. Tumors were resected 90

minutes after treatment with VEGFR inhibitor (i.v., 75 mg/kg motesanib on day 4). Each dot represents one independent tumor. All the p-values were assessed by unpaired Student's two-sample *t*-test.

Figure 5. Tumor cell-derived COX-1 metabolites are required to induce Ca^{2+} transients and locally promote tumor immune evasion

(A, B) The dynamics of intracellular Ca^{2+} concentration *in vivo* was visualized in parental melanoma, *Ptgs1/Ptgs2*$^{-/-}$ melanoma, *Ptgs1*$^{-/-}$ melanoma, and *Ptgs2*$^{-/-}$ melanoma cells. Each image represents the fold increase in fluorescence intensity over 10 minutes. Each dot represents the proportion of Ca^{2+} transient-positive cells in an individual mouse (data from 3 to 5 mice per group). (C) The experiments were conducted in a similar fashion as the experiments in (A) and (B). The dynamics of intracellular Ca^{2+} concentration was visualized in *Ptgs1/Ptgs2*$^{-/-}$ melanoma cells implanted with parental melanoma cells contralaterally or ipsilaterally. Each image represents the fold increase in fluorescence intensity over 10 minutes. Each dot represents the proportion of Ca^{2+} transient-positive cells in an individual mouse (data from 3 mice per group). (D) Transcriptional activity of NFAT was assessed by an Akaluc luciferase-based reporter assay 4 days after implantation. Each dot represents the bioluminescence intensity of an individual tumor. When needed, a COX inhibitor was injected for 4 days (i.p., 25 mg/kg flurbiprofen axetil, daily from day 0). The expression of the reporter gene was regulated by a NFAT-driven promoter or CAG promoter. (E) C57BL/6NCrSlc mice were inoculated with 2 x10^5 parental and *Ptgs1/Ptgs2*$^{-/-}$ or *Gnaq*$^{-/-}$ melanoma cells contralaterally. Each line represents the growth of an individual tumor inoculated in mice. Data represent one of two independent experiments with 4 to 5 mice per group. All the p-values were assessed by unpaired Student's two-sample *t*-test.

Figure 6. VEGF receptor signaling plays a pivotal role in tumor cell-derived PGE_2 secretion mediated by host cell-derived TXA_2, thereby promoting tumor immune evasion

VEGF receptor signaling increases intra-tumoral TXA_2 concentration derived from host cells. TXA_2 binds to TP on tumor cells, which triggers Gq-mediated Ca^{2+} transients and PGE_2 secretion from tumor cells, resulting in the evasion of anti-tumor immunity. COX-1 expression is required for Ca^{2+} transients in melanoma cells *in vivo*, suggesting that PGE_2 secretion from tumor cells also enhances TXA_2 release from host cells.

Supplementary Files

Figure 1. Cas9 expression has limited influence on anti-tumor immunity, related to Figure 2

(A) The proliferative capacities of parental and *Gnaq*$^{-/-}$ melanoma cells *in vitro* were analyzed by cell counting for 5 days. Each line represents an individual cell line. The average number of cells at day 0 was normalized to 1 and cell proliferations were presented as the normalized values. Data represent the averaged value of 4 independent experiments for each cell line. (B) C57BL/6NCrSlc mice were inoculated with 2 x10^5 parental melanoma cells with or without Cas9 expression. Each line represents the growth of an individual tumor inoculated in mice. Data represent one of two independent experiments with 4 mice per group. The size of tumors formed by parental melanoma cells with or without Cas9 expression, *Gnaq*$^{-/-}$ melanoma cells, and *Gnaq*$^{-/-}$ melanoma cells introduced with Gnaq (*Gnaq*$^{-/-}$ + Gnaq) was analyzed. Some of the samples were the same as in Figure 2C. Each dot represents an individual mouse. Data represent the sum of two independent experiments with 8 mice per group. All the p-values were assessed by unpaired Student's two-sample *t*-test.

Figure 2. The GqPCR signaling pathway is required for tumor immune evasion in 4T1 breast tumor, related to Figures 1 and 2.

(A) The dynamics of intracellular Ca^{2+} concentration *in vivo* was visualized in parental 4T1 breast cancer cells, 15 minutes after injection of YM-254890 (i.v., 0.6 mg/kg), and *Gnaq*$^{-/-}$ 4T1 breast cancer cells. Each image represents the fold increase in fluorescence intensity over 10 minutes. Each dot represents the proportion of Ca^{2+} transient-positive cell in an individual mouse (data from 3 or 4 mice per group). (B) BALB/c mice and BALB/c *nu/nu* (nude mice) were inoculated with 2 x10^5 parental or *Gnaq*$^{-/-}$ melanoma cells. Each line represents the growth of each tumor inoculated in mice. Data represents one of two independent experiments with 4 mice per group. All the p-values were assessed by unpaired Student's two-sample *t*-test.

Figure 3. COX inhibition suppresses Ca^{2+} transients in melanoma cells *in vivo*, related to Figure 3.

(A, B) Dynamics of intracellular Ca^{2+} concentration *in vivo* was visualized in parental melanoma treated with COX inhibitor (i.v., 25 mg/kg flurbiprofen axetil). Each image represents fold increase in fluorescence intensity over 10 minutes before and 60 minutes after drug treatment. Each line represents an individual mouse experiment. All the p-values were assessed by unpaired Student's two-sample *t*-test.

Figure 4. TXA_2 mimetic I-BOP triggered Ca^{2+} transients in melanoma cells under *in vitro* conditions, related to Figure 3.

(A) Parental and *Tbxa2r*$^{-/-}$ melanoma cells expressing GCaMP6s were time-lapse imaged under *in vitro* conditions. To stimulate the TP receptors, 10, 100, and 500 nM I-BOP was added to the media every three minutes. Representative fluorescence intensity images of GCaMP6s after each stimulation were shown. The fluorescence time course of GCaMP6s in representative cells were quantified as the fold increases in fluorescence intensity at each time point to fluorescence intensity of minimum intensity projection over 16 minutes. Data from three representative cells from each group of cells responded to 100 nM I-BOP (red), responded to 500 nM I-BOP (blue), and not responded to 500 nM I-BOP (green). The fluorescence intensity was measured by averaging all pixels within the region of interest (ROI) in each cell. Representative from three independent experiments with similar results.

Figure 5. Depletion of infiltrating host cells had little effect on Ca^{2+} transients in melanoma cells, related to Figure 4.

(A-B) The dynamics of intracellular Ca^{2+} concentration *in vivo* was visualized in parental melanoma cells. Parental melanoma cells were inoculated into either C57BL/6NCrSlc (wild

type) or NOG mice treated with the following reagents: platelet-depleting antibody (R300, anti-CD42b (GPIbα), i.v. at day 0 and day 1), NK cell-depleting antibody (α-asialo GM1, i.p. at day -1 and day 0), Ly6G-positive neutrophil-depleting antibody (α-Ly6G, i.p. every other day from one day -1), and macrophage-depleting drug (clodronate, i.p. from day -3 to day -1). Each image represents the fold increase in fluorescence intensity over 10 minutes. Each dot in the graph represents the proportion of Ca^{2+} transient-positive cells in an individual mouse (data from 3 mice per group). (C) Secretion of TXA_2 from HUVECs stimulated by 100 ng/ml VEGF was measured by ELISA for TXB_2. When needed, 100 nM motesanib, VEGF receptor antagonist, was added. All the p-values were assessed by unpaired Student's two-sample *t*-test.

Table 1. The list of mice employed for ELISA analysis, related to Figure 2, Figure 3, and Figure 4.

Total 28 mice were employed for ELISA analysis. The table provides the information on melanoma cells implanted, drugs administrated, the date when tumors were resected, the weight of tumor tissues (mg), and the weight of PGE_2 (w/w $x10^{-6}$) or TXB_2 (w/w $x10^{-9}$).

Video 1.

Live imaging of MDCK cells expressing the PKA biosensor. $Braf^{V600E}$ melanoma cells expressing the DREADD hM_3 were stimulated by 1 μM CNO treatment at 60 seconds. PKA activation in surrounding MDCK cells was observed 30 seconds after stimulation. Scale bar = 100 μm. Times are shown in minutes (m) and seconds (s).

Video 2.

Live imaging of $Braf^{V600E}$ melanoma cells expressing GCaMP6s *in vivo* and *in vitro*. Pseudo colors represent the fluorescence intensity as in Figure 1C. Images were acquired every 6 seconds for 20 minutes. A small population of tumor cells continuously shows active Ca^{2+}

transients repeatedly *in vivo*, but not *in vitro*. Scale bar = 60 μm. Times are shown in minutes (m) and seconds (s).

Video 3.

Intravital imaging of $Braf^{V600E}$ melanoma cells expressing GCaMP6s. Images represent the fold increase in fluorescence intensity shown in IMD mode as in Figure 1E. Images were acquired every 3 seconds for 15 minutes. From left to right: parental melanoma, $Gnaq^{-/-}$ melanoma, and $Gnaq^{-/-}$ melanoma cells introduced with Gnaq ($Gnaq^{-/-}$ + Gnaq). Genetic ablation of *Gnaq* abolished active Ca^{2+} transients observed in parental cells, which was restored by the introduction of Gnaq in $Gnaq^{-/-}$ melanoma. Scale bar = 60 μm. Times are shown in minutes (m) and seconds (s).

Video 4.

Intravital imaging of $Braf^{V600E}$ melanoma cells expressing GCaMP6s with or without treatment of a VEGFR inhibitor, motesanib. Images represent the fold increase in fluorescence intensity shown in IMD mode as in Figure 4C. Images were acquired every 6 seconds for 40 minutes. Motesanib was intravenously administered at 10 minutes. At only about 20 minutes after administration, the Ca^{2+} transients were significantly suppressed. Scale bar = 60 μm. Times are shown in minutes (m) and seconds (s).

Figure 1. The GqPCR signaling pathway triggers Ca^{2+} transients in melanoma cells to generate PGE_2 in vivo.

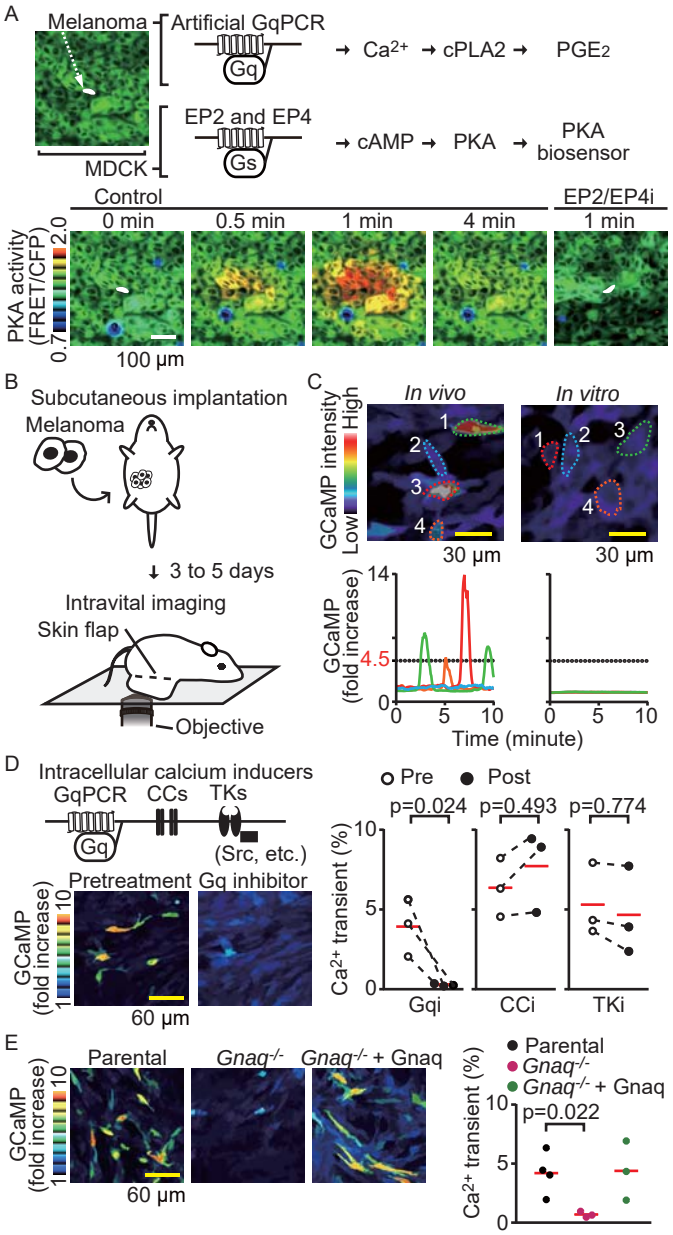

Figure 2. The GqPCR signaling pathway is required for PGE_2 secretion and tumor immune evasion.

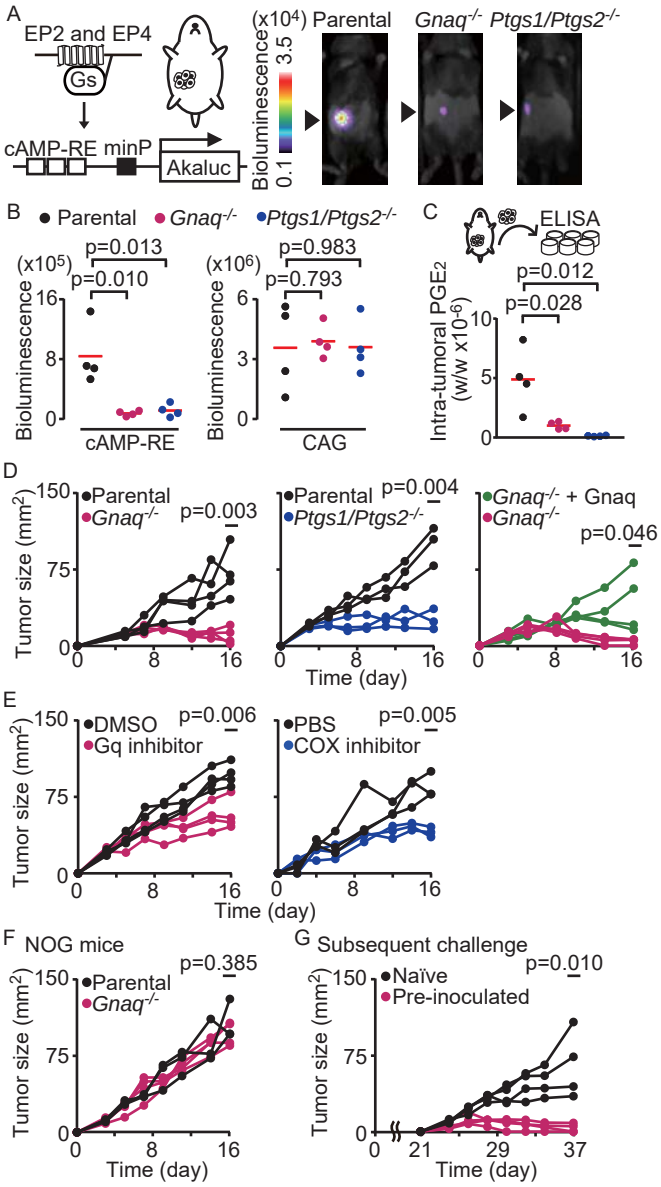

Figure 3. TXA_2-TP signaling triggers Ca^{2+} transients for PGE_2 secretion and tumor immune evasion in vivo.

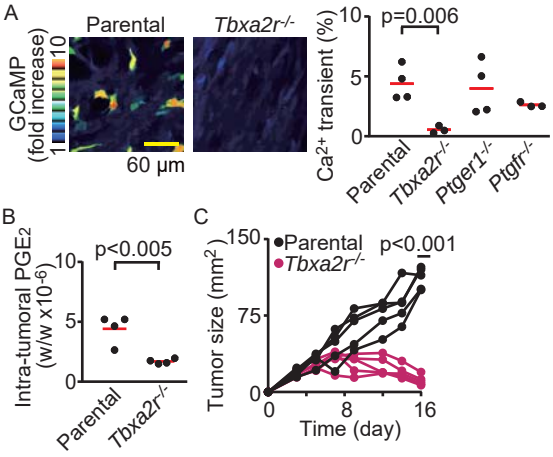

Figure 4. VEGF receptor signaling is indispensable for TXA_2 mediated PGE_2 secretion.

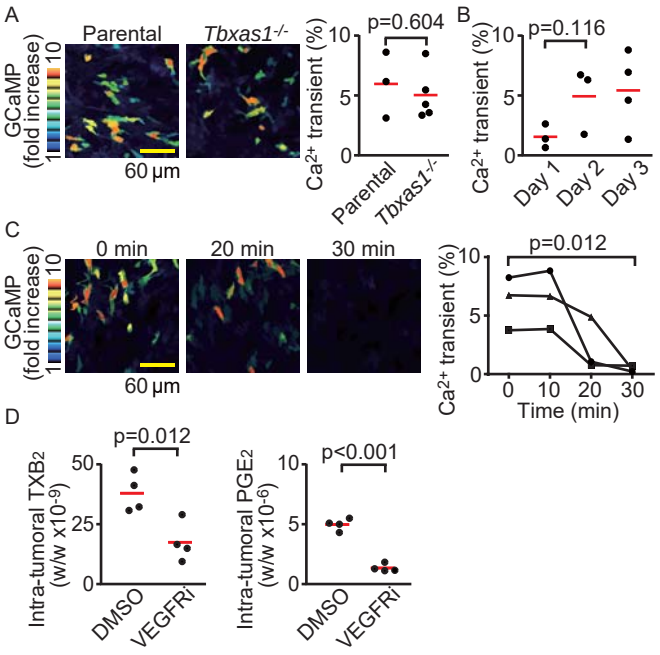

Figure 5. Tumor cell-derived COX-1 metabolites are required to induce Ca^{2+} transients and locally promote tumor immune evasion.

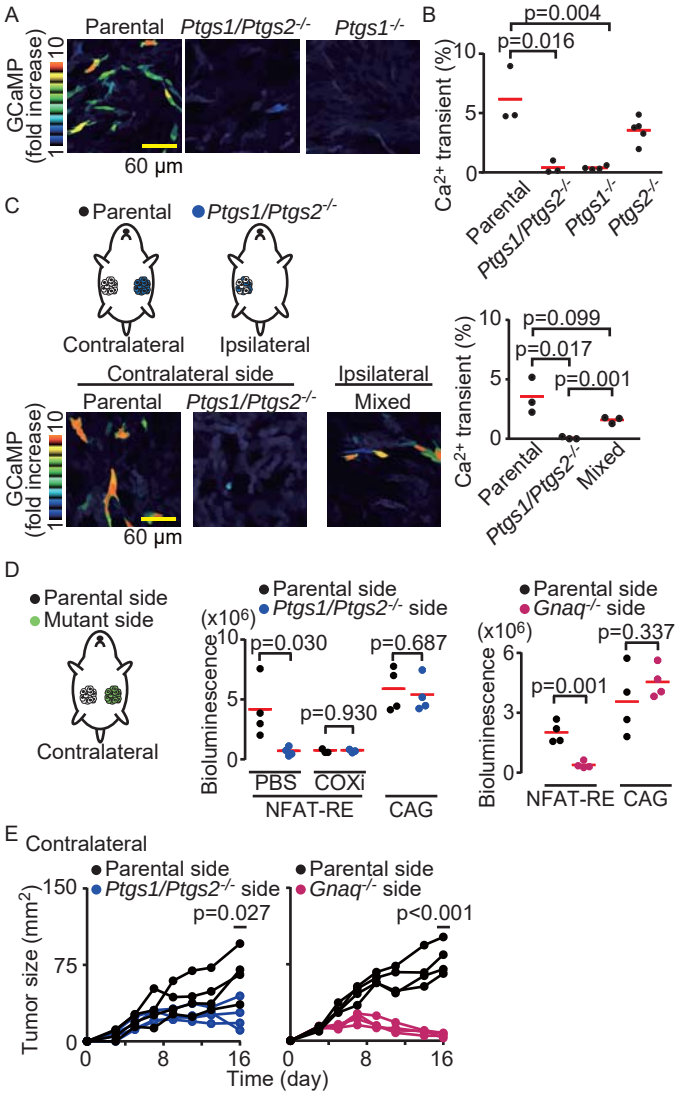

Figure 6. VEGF receptor signaling plays a pivotal role in tumor cell-derived PGE_2 secretion mediated by host cell-derived TXA_2, thereby promoting tumor immune evasion.

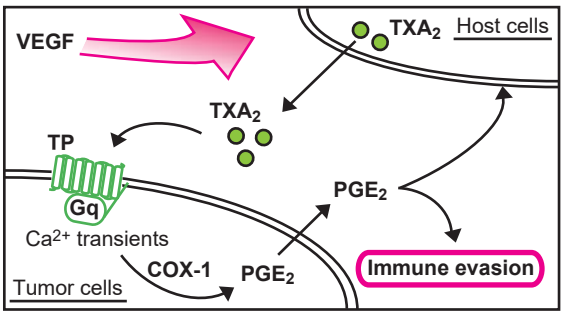

Table 1. The list of mice employed for ELISA analysis, related to Figure 2, Figure 3, and Figure 4.

Total 28 mice were employed for ELISA analysis. The table provides the information on melanoma cells implanted, drugs administrated, the date when tumors were resected, the weight of tumor tissues (mg), and the weight of PGE_2 (w/w $x10^{-6}$) or TXB_2 (w/w $x10^{-9}$).

Melanoma	Mouse	Sample collection	Drug	Weight of tumors (mg)	Wight of PGE_2 (w/w $x10^{-6}$)
Parental	#1	16 October 2020	N/A	30.1	5.1
	#2	16 October 2020	N/A	23.0	1.7
	#3	16 October 2020	N/A	14.0	8.2
	#4	16 October 2020	N/A	15.5	4.5
	#5	20 November 2020	N/A	21.0	4.6
	#6	20 November 2020	N/A	16.8	2.6
	#7	20 November 2020	N/A	16.2	5.2
	#8	20 November 2020	N/A	20.4	5.2
	#9	1 December 2020	DMSO	15.9	5.1
	#10	1 December 2020	DMSO	25.8	5.5
	#11	1 December 2020	DMSO	12.1	4.3
	#12	1 December 2020	DMSO	20.1	5.0
	#13	1 December 2020	Motesanib	14.5	1.2
	#14	1 December 2020	Motesanib	28.7	1.1
	#15	1 December 2020	Motesanib	21.3	1.3
	#16	1 December 2020	Motesanib	20.2	1.8
***Ptgs1/Ptgs2*$^{-/-}$**	#17	16 October 2020	N/A	22.5	0.2
	#18	16 October 2020	N/A	11.8	0.1
	#19	16 October 2020	N/A	16.2	0.1
	#20	16 October 2020	N/A	22.3	0.1
***Gnaq*$^{-/-}$**	#21	16 October 2020	N/A	23.8	0.7
	#22	16 October 2020	N/A	17.0	1.2
	#23	16 October 2020	N/A	12.7	0.8
	#24	16 October 2020	N/A	18.2	1.3
***Tbxa2r*$^{-/-}$**	#25	20 November 2020	N/A	15.6	1.6
	#26	20 November 2020	N/A	16.4	1.8
	#27	20 November 2020	N/A	19.6	2.0
	#28	20 November 2020	N/A	12.6	1.5

Melanoma	Mouse	Sample collection	Drug	Weight of tumors (mg)	Wight of TXB_2 (w/w $x10^{-9}$)
Parental	#9	1 December 2020	DMSO	15.9	32
	#10	1 December 2020	DMSO	25.8	31
	#11	1 December 2020	DMSO	12.1	41
	#12	1 December 2020	DMSO	20.1	48
	#13	1 December 2020	Motesanib	14.5	29
	#14	1 December 2020	Motesanib	28.7	17
	#15	1 December 2020	Motesanib	21.3	9
	#16	1 December 2020	Motesanib	20.2	15

Supplementary figure 1. Cas9 expresson has limited influence on anti-tumor immunity, related to Figure 2.

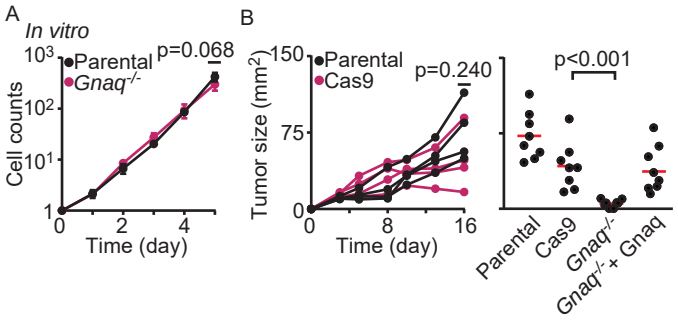

Supplementary figure 2. The GqPCR signaling pathway is required for tumor immune evasion in 4T1 breast tumor, related to Figure 1 and 2.

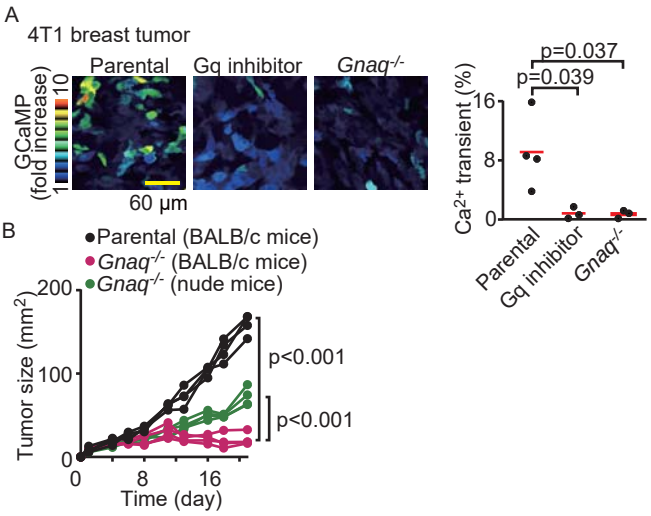

Supplementary figure 3. COX inhibition suppresses Ca^{2+} transients in melanoma cells in vivo, related to Figure 3.

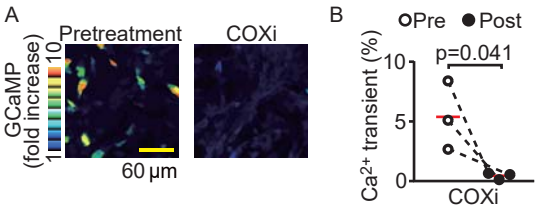

Supplementary figure 4. TXA_2 mimetic I-BOP triggers Ca^{2+} transients under in vitro conditions, related to figure 4.

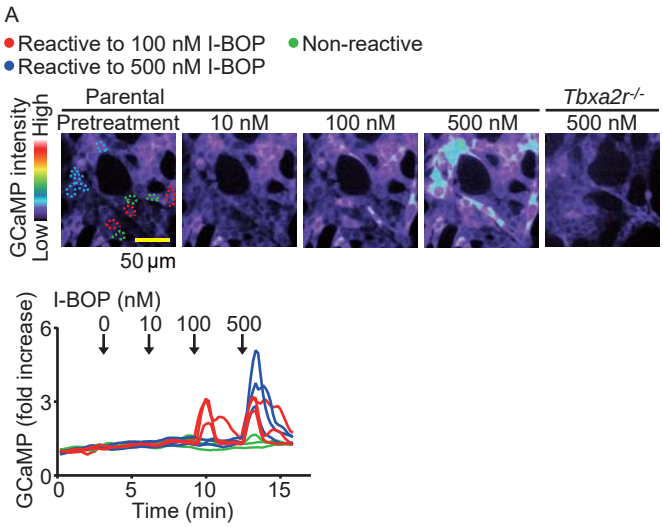

Supplementary figure 5. Depletion of infiltrating host cells has little effect on Ca^{2+} transients in melanoma cells, related to Figure 4.